PRESSURE DISTRIBUTION ON AN UNDERTURNING ICE FLOE

Barry Coutermarsh and W. Randy McGilvary
U.S. Army Cold Regions Research and Engineering Laboratory
72 Lyme Road
Hanover, New Hampshire 03755-1290, U.S.A.
(603) 646-4100

Abstract

This paper describes an experimental study to measure the dynamic fluid pressure beneath a floating parallelepiped block. Calculations show that this fluid pressure is by itself sufficient to start a block rotating from a horizontal position and that the underturning moments tend to increase during rotation.

Tests were run at various flow velocities, flow depths and block angles of attack. Results show that pressure magnitude and distribution is dependent not only upon flow velocity but also on flow depth and angle of attack. A flow reduction ratio which includes the thickness-to-depth ratio, the length-to-depth ratio, and the block angle of attack is introduced. The relationship between moment coefficient and flow area reduction ratio suggests that length is as important as thickness when investigating block stability in deep water conditions, particularly for blocks with high length/thickness aspect ratios.

An underturning moment is calculated for various water velocities, block angles of attack and flow depths. The propensity of a block to underturn is compared with the hydrostatic stabilizing moment caused by block submergence.

Key Words

Ice	Dynamic fluid pressure	Ice cover
Block underturning	Hydrostatic righting moment	
StabilityIce jams	Ice jams	

Introduction

Block underturning has been studied to help define both the initiation and progression of an ice cover. Ice floes that float downstream and come to rest against an obstruction, such as an ice boom or an intact ice sheet, will either remain there or underturn. Floes that do not underturn become part of an ice cover that progresses upstream, while floes that underturn may become lodged beneath any downstream cover and contribute to the growth of a hanging dam. It is for these reasons that it is important to understand the conditions that affect ice floe stability. A schematic diagram of the physical situation and variables is shown in figure 1.

For purposes of calculating ice block underturning stability, most of the previous work has assumed that the block rotates about its lower downstream corner. We have followed this convention in order to calculate both block buoyancy and underturning moments.

Numerous studies have been performed to describe a block stability criteria. Most, however, have assumed simple empirical descriptions for the forces and moments caused by fluid acceleration around the floating block. In this study the actual pressures acting on the bottom surface of a floating block were measured for various conditions of flow velocity, flow depth and block angle of attack. These measured pressures were both positive (stabilizing) and negative (destabilizing), depending primarily upon the angle of attack. The resulting integrated force magnitude and center of pressure locations were used to calculate the total resultant underturning moment acting on the block. In order to simplify the analysis we did not include the higher order dynamic pressures associated with the fluid added mass, block rotational inertia and the changing relative velocity between

the fluid and the block by using a rigidly supported block. Several representative three-dimensional surface plots of pressure at various block angles of attack are presented.

A hydrostatic analysis of the block's buoyancy-induced righting moment as a function of attack angle was compared with the measured underturning moment to determine when the block would underturn.

Background

Most investigators of block stability have relied upon the assumption of a uniformly distributed underturning pressure across the block and asserted the simplifying "no-spill" criterion to determine the point at which a block would underturn. They confounded the situation further by performing static analyses on data which included block angular acceleration and angular velocity.

Confusion has been most evident in detailing the point at which the block actually becomes unstable and underturns. It appears the most popular point of view seems to be that presented by Pariset and Hausser (1961). In this paper the point of instability is implicitly assumed to be when the upstream edge of an ice floe becomes submerged. This situation was called the "no-spill" condition in later papers.

Ashton (1974) employed the "no-spill" criterion and declared a vital dependence upon block thickness and block thickness-to-depth ratio but believed that thickness-to-length was of little importance, as was depth alone. He also provided a simplified moment analysis taking into account the block weight, the global fluid acceleration to maintain continuity, and the displaced volume of fluid.

Larsen (1975) presented a theoretical pressure distribution beneath a block with a rounded upstream face based upon potential flow theory. He showed the lowest pressure at the front of the block rising exponentially towards the rear. A comparison between block Froude numbers at underturning, determined experimentally, with those predicted

by the theory showed fair agreement between the two. In the range of depths that he studied, the critical velocity for underturning was not dependent upon depth. Both Larsen and Uzuner and Kennedy (1972) mentioned the importance of the local flow behavior around the block in creating underturning forces but did not characterize them.

Daly and Axelson (1990) performed a detailed calculation to determine the hydrostatic righting moment related to the displaced volume of the block as it rotates. This righting moment was found to peak at an angle depending on fluid density, block density, thickness and length. They reasoned that block instability was reached when the underturning moment due to the fluid flow was greater than the righting moment which discounted the previous notion of the "no-spill" condition. Their analysis also determined a moment coefficient that included two empirically determined parameters found through investigation of the existing laboratory data.

Experimental Objective

The object of this study was to experimentally measure the pressure caused by local fluid acceleration beneath an idealized ice block. The two-dimensional pressure distributions beneath the block were measured for three block thickness-to depth-ratios at various flow velocities and block angles of attack. The average pressure and center of pressure were calculated and used to calculate underturning moments. The underturning moments were compared with the block's buoyancy-induced righting moment up through the maximum buoyancy angle of attack.

Experimental Setup

The experiments were performed in a flume with cross-sectional dimensions of 0.91 meter by 0.91 meter, a total length of 7.32 meters, and a variable pumping capacity up to 0.3 m^3/s. A 61.6-cm-square, 7.62-cm-thick hollow Plexiglas "ice floe" was constructed

with 91 pressure taps in its bottom surface. The taps were sized to accept 6.35-mm-OD polyethylene manometer tubing and were variably spaced as shown in figure 2. A Plexiglas cover extended over the top front half to prevent water from impacting against the tubes as the block front submerged during rotation. The block was fastened to the flume by hinged supports at its rear and an adjustable threaded rod at its front top as shown in figure 3. This allowed both vertical and rotational (angle of attack) adjustments.

Pressure measurements were accomplished by routing 24 water-filled manometer tubes via a fluid switch multiplexer to a ± 6.35-cm-range, liquid-to-gas, pressure transducer. In this manner it was possible to measure 24 separate manometer taps with one transducer. A stilling tube gave us a stable measure of the piezometric head in the flume, which was measured at the beginning and end of each group of readings. In this way the dynamic fluid pressure difference from static was determined for each tap. The readings and their standard deviations were plotted real-time and stored on a personal computer.

Test Procedure

A typical test started by setting the water to the desired depth and submerging the block to the required displacement. The flume velocity was adjusted to the desired value and two scans of 25 pressures (two for static height and 23 taps) were made. The model floe was rotated to the next desired angle and two more scans performed. This procedure was repeated until all desired block angles were completed for any given depth and velocity.

The experiments were performed in two phases. The first phase was to verify the symmetry of the pressures across the full width of the block. The second phase was to measure pressures on one half of the block, assuming symmetry of the pressure distribution for the other half.

Results

Phase One

A typical pressure distribution obtained during phase one of our experimental program is shown in figure 4. The x-axis is block width, the y-axis length (up to 18 cm from the leading edge of the block) and the z-axis is in pascals. The water flow was in the positive y direction. The readings were obtained at zero angle of attack and a velocity of 0.35 m/s. In these experiments a negative pressure tends to rotate the block downward, i.e. toward the negative z direction, and a positive pressure pushes against the block in the positive z direction. Examination of the figure points out the pressure distribution's high degree of symmetry about the block centerline at x = 30.5 cm. Indeed, the center of pressure in the x-direction was found to lie 1.23 cm from the centerline, and the moment about the centerline was 0.03 N–m. Having proven symmetry, we instrumented one half of the block along its entire length, and entered the second phase of the experimental program.

Phase Two

The experiments were run at three values of t/H: 0.10, 0.13 and 0.20, corresponding to a fixed block thickness of 7.62 cm and three different flow depths. Velocities used were 0.14, 0.23, 0.39, 0.45, 0.50 and 0.60 m/s. Block attack angles ranged from 00 to approximately 200. Two replicates were performed at each condition, except as noted in table 1, and the data presented are the average of these two replicates. We will show below some representative pressure plots that cover our t/H values and selected block angles of attack, at V = 0.45 m/s and 0.5 m/s. These distributions illustrate the patterns found in our experiments and show the variations found with increasing angle of attack and changing depth.

Figure 5 is a series of surface pressure plots from three tests: test 1: t/H= 0.10, V = 0.45 m/s ("deep water"); test 2: t/H = 0.13, V = 0.50 m/s; test 3: t/H = 0.20, V = 0.50 m/s

("shallow water"). Only three block angles of attack are illustrated here as shown. The axis of rotation for the attack angle and center of pressure measurements was at y = 0.0, which was the back lower edge of the block. The vertical z axis is pressure in pascals measured on one half of the block and numerically applied to the other half due to the symmetry demonstrated in phase one. Each line represents an isobar with a contour interval of 10 Pa. Following figure 3, negative pressure is a suction on the underside of the block and tends to both submerge and rotate it. Positive pressure pushes up against the block, tending to stabilize it by opposing the underturning moments generated by the negative pressure.

These pressure distributions are typical of the patterns found during phase two. Generally, at zero angle of attack, the pressures were lower and negative at the front of the block and becoming less negative, if not positive, where flow reattachment occurs, towards the rear of the block. The rear central portion of the block frequently experienced a slightly positive pressure, with some areas of negative pressure at the corners. The pressure at the front central portion of the block was usually less negative than the front sides or the block's midsection, leading to a characteristic "saddle" shape in the pressure distribution. As the angle of attack increased, the magnitude and area of negative pressure would increase, until the entire pressure distribution became negative. Correspondingly, the center of positive pressure moved towards the rear of the block. Visual observation indicated that at the higher angles of attack, the flow was separated over nearly the full block length, and few positive pressures were measured.

Because of the block geometry, flow separation is present at all times, removing any dependence on Reynolds number. In terms of the hydrodynamics, velocity changes have the primary effect of changing the pressure magnitude. The changes in the pressure distribution and location of flow reattachment are less sensitive to changes in velocity than changes in attack angle.

It can be seen in figure 5 that the distributions from test 1 (t/H = 0.10) tended to be more uniform between the front and rear sections of the block than those from tests 2 and 3 (t/H = 0.13 and 0.20 respectively). In test 3 the pressure difference between the front and rear sections of the block is greater and the overall pressure is lower. There are also numerous areas of extremely low pressure, probably associated with vortex formation and flow separation.

Analysis

Because the pressure distribution generally has positive and negative components, calculation of a single center of pressure is not entirely useful. Therefore, for the sake of characterizing the pressure distribution, we have considered the positive and negative pressure distributions separately. Separate calculations of surface area over which the pressure acts and the average pressure for regions of positive and negative pressure are shown graphically in figure 6. It is interesting that tests 1 and 3 have roughly the same area of negative pressure, with a much greater magnitude for test 3.

The area and magnitude of the pressures are not enough to determine when the block may underturn because of the assumption of rotation about the downstream lower edge. It is also necessary to use the center of the pressures to calculate moments about the rotation axis. Figure 7 shows the positive and negative center of pressure (COP) locations (measured from the rotation axis) and the resultant moment for each test. Here it can be seen that although test 2 did not have quite the area of negative pressure that test 1 did its negative COP is farther from the axis of rotation while its positive COP is about the same as test 1's. This results in the two moments being very similar in the initial stages of rotation, with test 2 being greater at the higher attack angles where the effect of depth is probably being felt. Test 3 has a much higher moment than the others but its negative COP is almost identical to test 1's. It should be noted that the positive COPs in tests 1 and 2 are

almost identical, while test 3's moves away from the rotation axis. This has the effect of hindering the block's rotation if we assume a pinned lower downstream corner.

In order to determine if the block is stable, we compare the measured moments due to dynamic fluid pressure with the block hydrostatic righting moments in figure 8. The righting moment is a function of block angle of attack and increases to a maximum at θ^* (Daly and Axelson 1991). The righting moment rises quickly to its maximum value, and slowly decreases, vanishing at an angle of $90 + \theta^*$ degrees. θ^* can be approximated by (Coutermarsh and McGilvary, in preparation):

$$\theta^* \approx \mathrm{Tan}^{-1}(t/L) \qquad [1]$$

For our block θ^* is 8.5 degrees, while the approximation gives 7.1 degrees.

Both the measured underturning moment and the righting moment are non-dimensionalized by the maximum righting moment, M_{max}, given by Coutermarsh and McGilvary (in preparation):

$$M_{max} \approx (1-r_i/\rho_w)\, \rho_w\, g\, t\, (A)\, L/2\,. \qquad [2]$$

It can be seen from figure 8 that the moments created on the block in the deeper water ($t/H = 0.10$ and $t/H = 0.13$) would not be sufficient to overcome the righting moment. At zero angle of attack the moment would start the block rotating, but at the next measured angle the moment is below the righting moment curve, which means it would be stable. Neglecting rotational inertia, the block is stable if the underturning moment is always less than the righting moment. In the shallow water ($t/H = 0.20$), however, the moments generated at every velocity of our experimental program would be sufficient to underturn the block.

In order to resolve the functional dependence of the underturning moment on the variables we have considered, we define a moment coefficient as:

$$\alpha = M / 1/2\, \rho_w V^2 (A)\, L\,. \qquad [3a]$$

An alternative definition of the moment coefficient is:

$$\alpha = C_\ell\, COP/L\,. \qquad [3b]$$

$$\text{where } C_\ell = \overline{P}/1/2\, \rho_w V^2\,. \qquad [4]$$

C_ℓ is the Euler number, often referred to as the lift or pressure coefficient, and $\overline{P}$ is the average pressure acting on the block. Figure 9 shows the moment coefficient as a function of attack angle for thickness-to-depth ratios of 0.13 and 0.20 and several velocities. Generally the moment coefficient increases with increasing attack angle. However, at t/H = 0.20, the coefficient increases more rapidly with angle than at t/H = 0.13, demonstrating the effect of flow constriction at shallower depths. A secondary effect is the general decrease in moment coefficient with increasing velocity. At a given angle of attack, the velocity effect is more pronounced in deeper flows than in shallower flows, as is evidenced by the larger spread in the data at t/H = 0.13.

As for all partially submerged structures, a combination of Reynolds number and Froude number is required to characterize the flow. Since the flow is separated for all the cases considered, we feel that the moment coefficient is relatively independent of Reynolds number. However, we have had limited success in characterizing both deep and shallow water data sets with a single Froude number. This may be in part due to wall effects, which were found to be small for deeper, lower velocity flows at 0°, but were never quantified for shallower, higher velocity flows at different angles of attack.

If we consider the depth of flow beneath the block, h, in relation to the upstream depth of flow, H, we arrive at a value similar to an orifice area reduction ratio:

$$h/H = 1 - (\rho_i/\rho_w)\,(t/H) - (L/H)\,\sin(\theta)\,. \qquad [5]$$

The flow area reduction ratio has all the fundamental groupings of interest, including the density ratio, thickness to depth ratio, length-to-depth ratio, and angle of attack. As is seen in figure 10, the moment coefficient is relatively linear with the area reduction ratio, with a slight scatter due to velocity effects. Such a relationship suggests that block length is at least as important as thickness for characterizing block stability for deep water conditions, especially for blocks with high L/t aspect ratios of about 10.

Conclusions and Recommendations

The hydrodynamic fluid pressures beneath an idealized, parallelepiped model ice block were measured. The ice block was fixed in space, thereby eliminating angular acceleration during measurement of the fluid pressures. The pressure distribution was shown to be symmetric about the centerline of the block and included regions of positive (stabilizing) pressure, and negative (underturning) pressure. The net underturning moment for the entire pressure distribution was compared with the hydrostatic righting moment, and the condition of static stability was described. A flow area reduction which includes the thickness-to-depth ratio, the length-to-depth ratio, and the angle of attack is presented. The moment coefficient appears to have a linear relationship with the reduction ratio over the range of parameters investigated. This linear relationship suggests that block length is as important as thickness for characterizing block stability in deep water conditions, especially for high L/t aspect ratio blocks.

The measured areas of positive pressure at the back of the block suggest that it is possible for a block to be pushed out of the water vertically at its downstream edge. Researchers we have spoken with have confirmed seeing this phenomena (G. Ashton 1991; J. Lever 1991).

There are several areas of the current study that could be expanded upon in future work. First, our study considered only one block geometry. Because of the three-dimen-

sional nature of the flow, other block thickness-to-length ratios and widths should be investigated. Consideration of blocks with rounded leading edges might also prove interesting to see the variation in flow attachment. Better flow visualization may also shed light on the phenomenon of positive pressures beneath the block.

Secondly, deep water data ($t/H > 0.10$) at velocities over 0.45 m/s could prove interesting. We were restricted in both available depth and achievable velocities in our facilities. We therefore could not fully characterize the deeper flows.

Finally, our experiments did not include any effect due to the dynamic fluid impact against the front and top of the block. Experiments that measure force on the block at a known distance from the assumed rotation point would contain this information although they would not reveal the nature of the forces. A simplified determination of block stability would allow more blocks and flow conditions to be analyzed in a given time, and would require less complex instrumentation and data reduction.

Acknowledgments

The authors wish to thank Dr. Eugene Marvin at CRREL for facilitating the funding of this work. Excellent in-house reviews were given by Dr. J.-C. Tatinclaux and Dr. James Lever. Credit is also due Dr. Lever for his suggestion of "h" as a more representative length scale for this particular work.

References

Ashton, G. D. (1974). Froude criterion for ice block stability. Journal of Glaciology, Vol. 13, No. 68, pp. 307–313.

Daly, S. and Axelson, K. (1990). Stability of floating and submerged blocks. Journal of Hydraulic Research, Vol. 28, No. 6, pp. 737–752.

Larsen, P. (1975). Notes on the stability of floating ice blocks. Proceedings of the Third International Symposium on Ice Problems, Hanover, N.H., International Association of Hydraulic Research, pp. 305–313.

Pariset, E. and Hausser, R. (1961). Formation and evolution of ice covers on rivers. Transactions of the Engineering Institute of Canada, Vol. 5, No. 1, pp. 41–49.

Uzuner, M. and Kennedy, J. (1972). Stability of floating ice blocks. Journal of the Hydraulics Division, American Society of Civil Engineers, Vol. 98, No. HY12, pp. 2117–2133.

Notation

A	Block planform area
C_ℓ	Lift coefficient, or Euler number
g	Acceleration due to gravity
H	Flow depth upstream from the block
h	Flow depth beneath upstream edge
L	Block length
$\overline{P}$	Average pressure
M	Underturning moment created by fluid flow
M_{max}	Maximum hydrostatic righting moment
t	Block thickness
V	Fluid velocity upstream from the block
x	Spatial coordinate, distance across block width
y	Spatial coordinate, distance along block length
z	Spatial coordinate, distance perpendicular to x–y plane
a	Nondimensionalized underturning moment (moment coefficient)
ρ_i	Ice density
ρ_w	Water density
θ	Block angle of attack (rotation) from horizontal

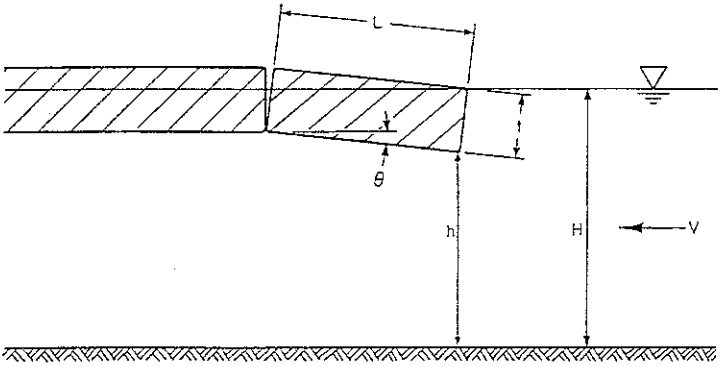

Figure 1. Physical and variable definitions for an underturning block.

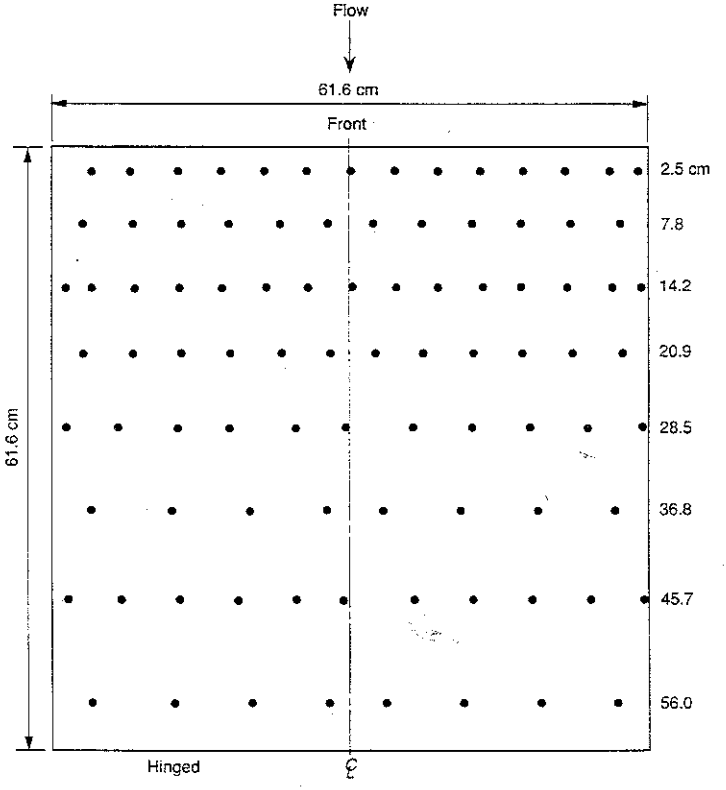

Figure 2. Dimensions and variably spaced tap locations on block bottom face.

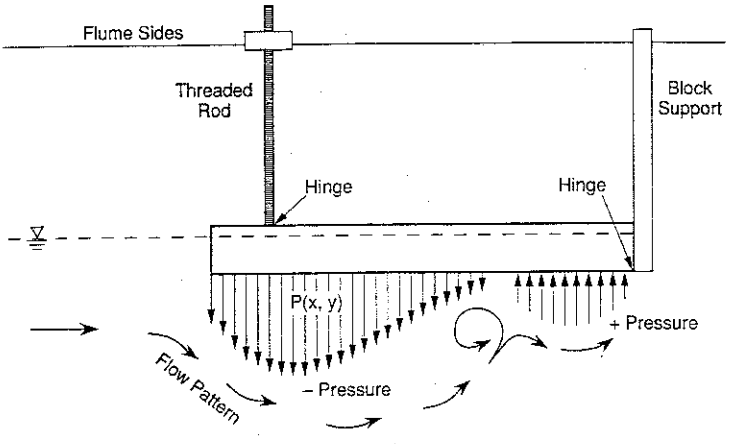

Figure 3. Idealization of flow beneath the block.

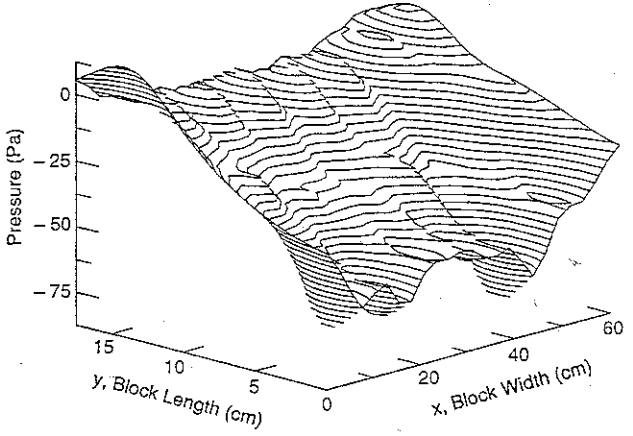

Figure 4. Pressure distribution measured in phase 1 across the full width of the block and from the front to 15 cm back. Visually, the distribution supports the assumption of symmetry. Integrating over the pressure distribution, the moment about the centerline is 0.03 N–m, and the center of pressure is 1.23 cm off the centerline.

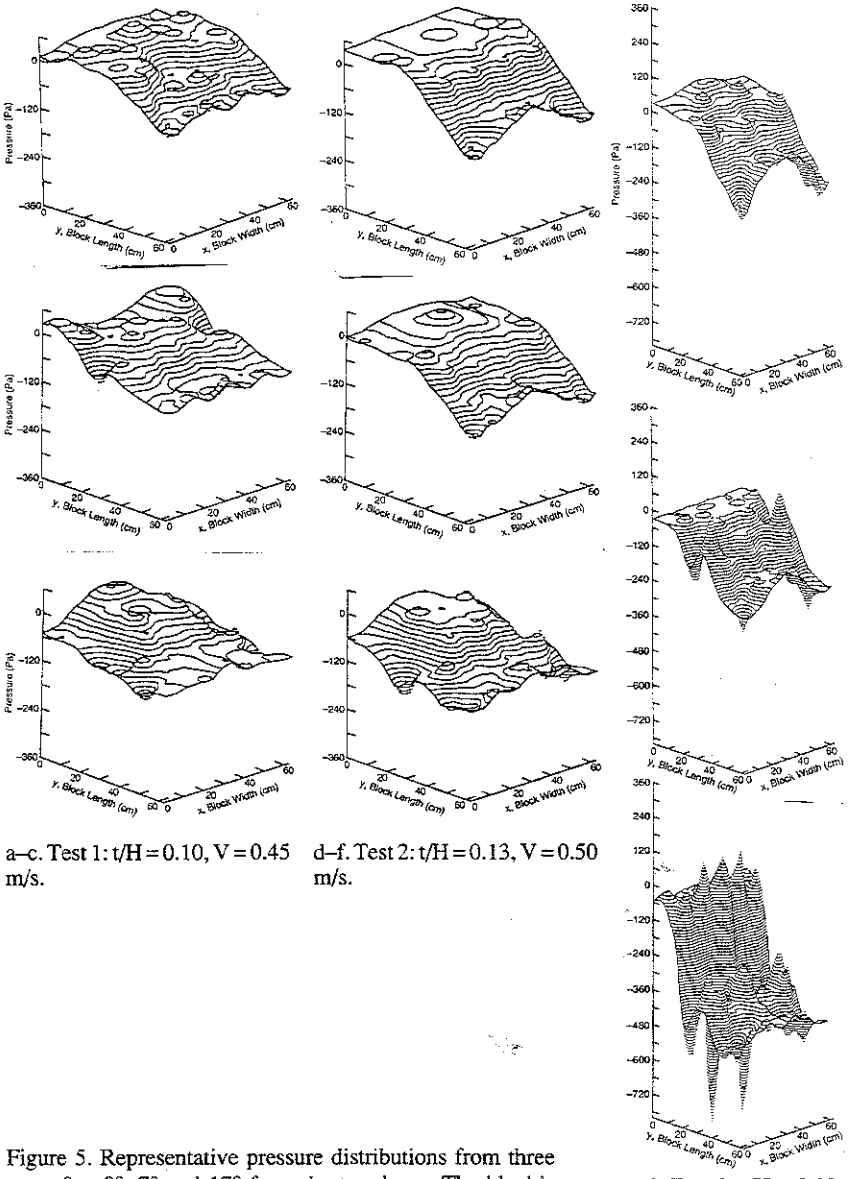

a–c. Test 1: t/H = 0.10, V = 0.45 m/s.

d–f. Test 2: t/H = 0.13, V = 0.50 m/s.

g–i. Test 3: t/H = 0.20, V = 0.50 m/s.

Figure 5. Representative pressure distributions from three tests. θ = 0°, 7° and 17° from the top down. The block's trailing edge is at y = 0.

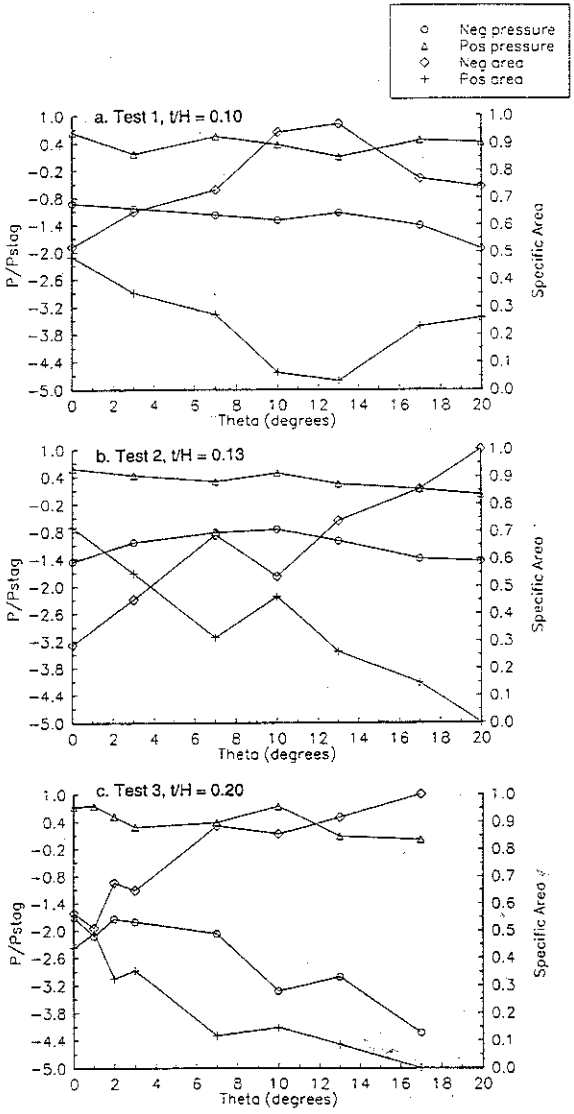

Figure 6. Areas of positive and negative pressure on the block's lower face nondimensionalized by the total block area. Also shown are the average pressures nondimensionalized with the stagnation pressure of the flow.

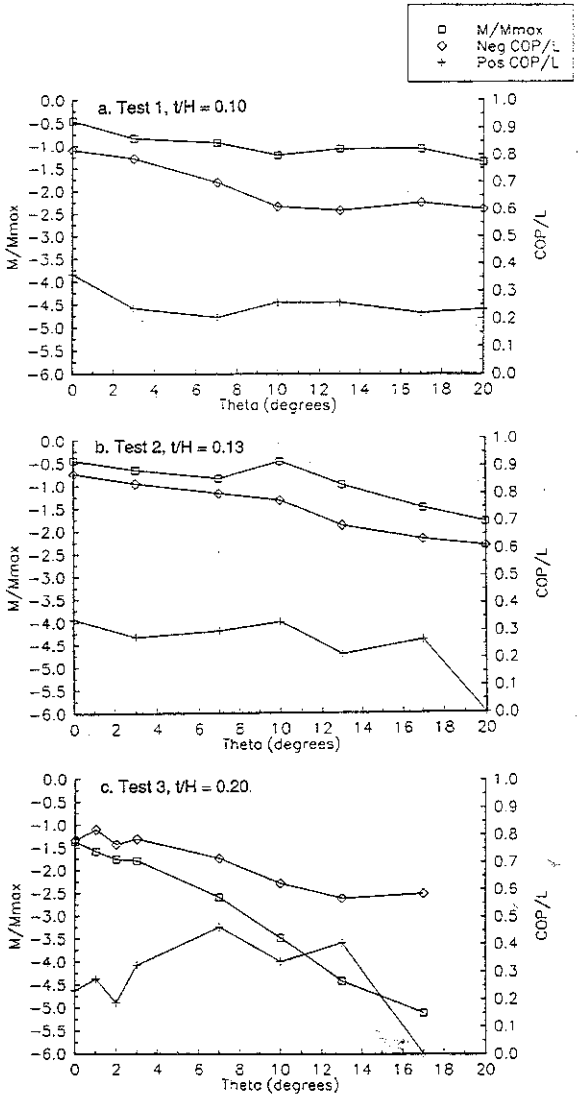

Figure 7. The center of negative and positive pressure divided by block length along with the total underturning moment nondimensionalized by the maximum hydrostatic righting moment. (COP/L = 0 is the axis of rotation).

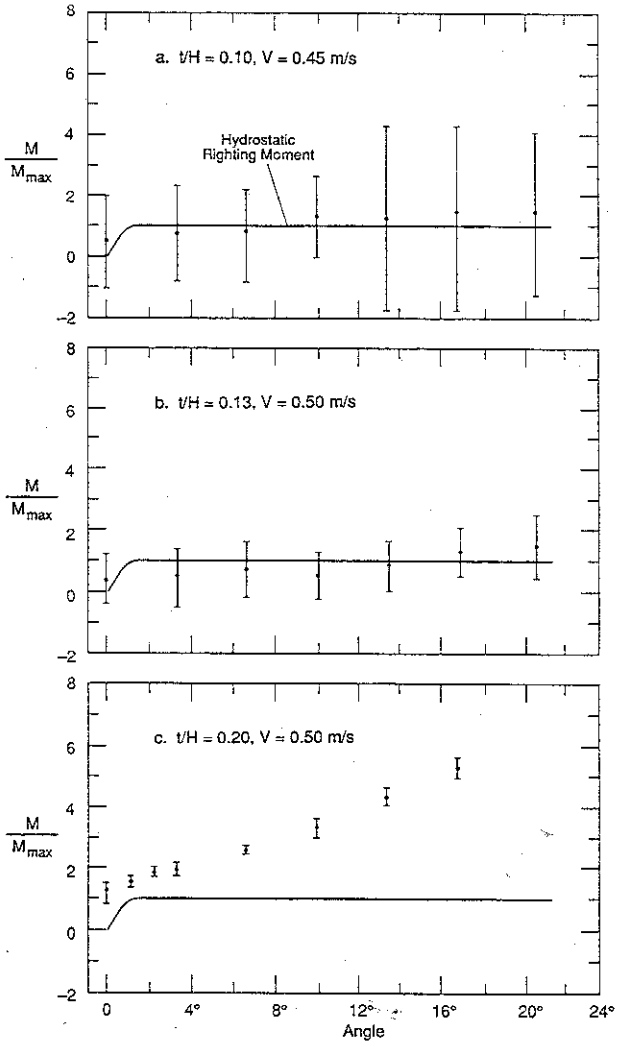

Figure 8. Nondimensional underturning moment versus block attack angle.

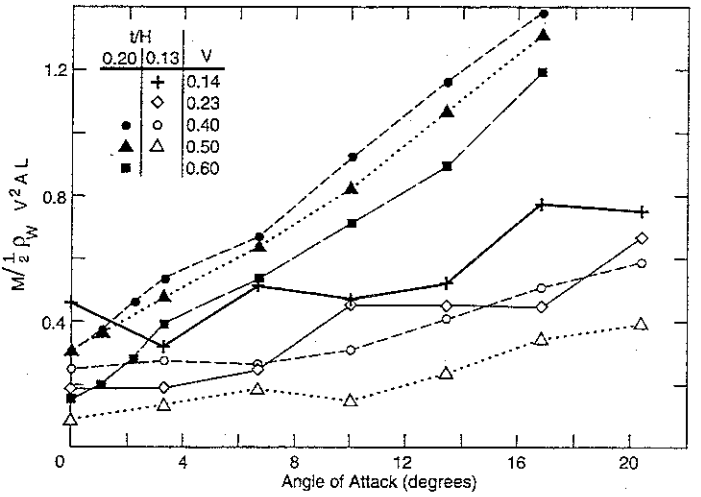

Figure 9 Moment coefficient versus angle of attack for t/H = 0.13 and t/H = 0.20 and several velocities.

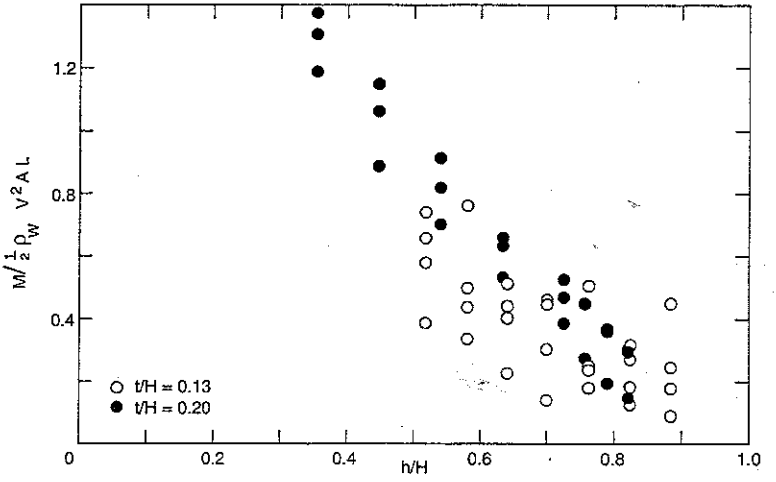

Figure 10. Moment coefficient versus h/H for all data. h/H represents an "area reduction ratio" for flow beneath the block.

Table 1. Test matrix showing thickness-to-depth ratios (t/H), velocities (V) and angles of attack.

t/H	Velocity V (m/s)				Angle of attack (degrees)			
0.10	0.45				0.0	3.3	6.6	10.0
					13.4	16.8	20.4	
0.13	0.14*	0.23	0.39	0.50	0.0*	3.3	6.6	10.0
					13.4	16.8	20.4	
0.20	0.39**	0.50	0.60		0.0**	1.1	3.3	6.6
					10.0	13.4	16.8	

* One test at t/H = 0.13, V = 0.14, and 0° angle of attack

** Four tests at t/H = 0.20, V = 0.39, and 0° angle of attack